

Ultrasound Thermometry for use in Tumor Ablation

Procedures

By

Timothy Sullivan Read

Thesis Advisor: Dr. Zbigniew Celinski; Department of Physics and Energy
Science, UCCS

Honors Representative: Dr. Daniel Dessau; Department of Physics, CU Boulder

Outside Reader 1: Dr. Kevin Manley, Department of Mathematics, CU Boulder

Additional Reader: Dr. Eric Burger, Program for Writing & Rhetoric, CU Boulder

A thesis submitted to the Faculty of the University of Colorado in partial
fulfillment of the requirements of departmental honors for the Department of

Physics

2022

To defend April 5th, 2022

Acknowledgements

This work would not have been possible without the dedicated work of my mentor Dr. Zbigniew Celinski, who put in countless hours to ensure that it met the high standards of our laboratory group. This work was also made possible by the dedicated community I had around me that offered me the support I sorely needed through a mentally tough year. Chief among these supporters is my mother, Dr. Mary Coussons-Read who offered me unparalleled and often undeserved support as I wrote this paper during a time in my life where it would have been smarter to leave it unwritten. Though it has been a rough process, I have been deeply touched by the amount of belief and support I have found in my community.

Contents

Introduction	1
1. Motivation.....	1
2. Overview.....	2
Background	3
1. Cancer and prostatectomy.....	3
2. Cryoablation.....	5
3. Laser ablation.....	7
4. Introduction to Ultrasound.....	10
5. Ultrasound thermometry.....	15
Methods	16
1. Design of an ultrasound thermometer.....	16
2. Setup.....	18
3. Homogeneous sample experiments.....	20
4. Inhomogeneous sample experiments.....	21
5. Probe modeling.....	22
Results & Conclusions	25
1. Homogeneous sample results.....	25
2. Inhomogeneous sample results.....	29
3. Probe modeling results.....	31
Conclusion	34
Future Work	35

Introduction

1.1 Motivation

A cancer diagnosis is often some of the most devastating and unsettlingly common news a patient can receive from a doctor; and with good reason, there are hundreds of different kinds of cancer that infect different areas of the body such as brain cancer, liver cancer, Leukemia, lung cancer, etc. all of which carry with them a significant chance of death and a near guarantee of hardship¹. The American Cancer Society estimates that in 2022 nearly 2 million new cancer cases have been diagnosed, and that over 600,000 patients have died in the United States alone². Yet not all cancers are equally deadly, of those 600,000 plus patients 78,000, had their lives taken by either breast or prostate cancers. The only cancer with a comparable kill count is lung cancer, making prostate and breast cancer two of the deadliest varieties that a patient might be diagnosed with^{2,3}. Making procedures and methods of treatment for these two varieties of cancer of particular interest to our society.

As detection methods for cancer have improved, surgical solutions have become more and more viable^{4,5,6}. Fortunately, unlike other cancers that make their homes on vital organs where such methods are extremely risky breast and prostate cancers are positioned in the body in places where surgery is viable⁷. This being said, traditional scalpel surgery is still quite unrefined and carries with it several extreme side effects that can last for a long time after the surgery itself, which is why alternative surgeries are more and more commonly employed to cure patients diagnosed with prostate and breast cancer^{7,8,9}.

Ablation procedures are a type of tumor removal process that employs thermal changes to destroy and remove malignant tissue, rather than using chemical, radiation, or mechanical

removal¹⁰. Such procedures offer a myriad of benefits to the patient as well as the physician, however, technological challenges related to thermometry methods can make such procedures difficult to perform safely^{11,12}. Without accurate, real time, temperature monitoring to guide ablation procedures, healthy non-malignant tissues are often destroyed causing a myriad of side effects¹³.

Currently, Magnetic Resonance Imaging (MRI) and Ultrasound are the two most popular platforms for providing guidance for ablation procedures¹⁴. While MRI provides many advantages such as higher resolution, high contrast in soft tissues, and the ability to take multi-planar cross-sections of an ablation site, it suffers from major issues namely, difficulties in obtaining real time imaging during a surgery, the physical challenges of performing a surgery in even an open design low-field MRI machines, and above all, expense¹⁵. Which is why Ultrasound is a more commonly used option as its relatively small probe size, capacity to take images of changing systems in real time, and low cost make it more accessible for a majority of surgeries¹⁶. However, the current methods of ultrasound employed, for example, by placing a probe in the rectum of a patient with prostate cancer, are far from perfect as it cannot make measurements of the heating or freezing volume around the ablation site.

1.2 Overview

This project aims to improve upon the current method of ultrasound guided ablation by designing and testing a concept of the invasive ultrasound probe to measure temperature. We envision that such a system will allow to monitor in real time and map temperature of the relevant flesh volume during an ablation procedure and to fit within a trocar needle already employed in such surgeries.

This design aims to achieve this by making use of the simple physical principle, that changes in temperature in a material often bring about changes in that material's resistance to compression. A sound wave can be thought of as a travelling compression, so as a material's temperature changes so too does its resistance to sound traveling through it¹⁷. If one knows the relationship between those changes in temperature and the subsequent changes in sound wave velocity, then it becomes easy to make an estimate of temperature using how far the sound must travel through a medium and the time it takes for it to do so. The proposed probe would take advantage of these facts by providing a system whose physical structure and sound velocity as a function of temperature are well known. Such a device would consist of several segments of homogeneous silicone polymer separated by acoustically resistant barriers. Discontinuity in material's acoustic properties would result in partial reflection and transmission of the ultrasound pulse generated by the ultrasound transducer¹⁸. By measuring the time of the reflected pulses sequence, an average temperature of a given segment can be determined based on the knowledge of its length and temperature-dependent sound velocity.

Background

2.1 *Cancer and Prostatectomy*

Cancer remains a major and unsolved problem in the world of medicine, with hundreds of thousands of lives being claimed by this family of diseases each year as mentioned above. Prostate cancer, often labeled as the most treatable form of cancer, still stands out as one of the deadliest¹⁹. The lives of thirty-four thousand US men were claimed by prostate cancer in 2021 alone, and two hundred and forty-eight thousand more received a diagnosis²⁰. The price tag for prostate cancer detection is staggering, costing the US healthcare system almost 1.2 billion dollars every three years²¹. Once diagnosed, patients with prostate cancer are faced with a choice between two types

of treatment, radiation therapy or surgery, each of which can produce challenges and side effects that are nearly as bad as the disease itself for some patients²².

Radiation therapy has long been a first line approach to the treatment of prostate cancer. It has a high survival rate and is often effective, especially in early-stage illness, but it is far from a perfect solution. Radiation therapy consists of subjecting a patient to high energy radiation daily for a period of one to two months²³. During this period and shortly afterwards patients often experience physical weakness, vomiting, diarrhea, headaches, hair loss, and a variety of other extreme side effects; side effects that often disappear after treatment but can remain for years in five percent of patients²⁴. Radiation therapy period patients may experience mental side effects such as long-lasting distress, anxiety, and depression which can continue after therapy has concluded²⁵. Short and long-term side effects are a major reason why, as detection methods for prostate cancer have improved and diagnosis occurs more commonly in early-stage cancers, many physicians have moved away from radiation therapy towards more aggressive surgical methods. Regrettably however, traditional surgical approaches do not produce significantly better therapeutic outcomes compared to radiation therapy.

Traditional surgical removal of a tumor is a daunting treatment for a prostate cancer patient, as it carries with it many risks as well as a large price tag. A typical prostatectomy, a surgery in which the prostate is either partially or fully removed, typically costs thirty-five thousand dollars. As with any surgery, complications on the surgical table may occur, yet the biggest risks with prostatectomy are the rates of long-term side effects. A traditional prostate surgery will unquestionably compromise the sexual function of a prostate cancer patient; nearly two-thirds of men who undergo the procedure will experience impotence for eighteen months or more after surgery and eight percent will be incontinent^{26,27}. There is little doubt that while the traditional

treatments for prostate cancer result in better outcomes than leaving the disease untreated, both options carry with them massive downsides. Fortunately for many patients, recently several promising alternative methods of surgical tumor removal are developing that reduce the chance of side effects substantially.

Thermal ablation is an alternative surgical approach for removing a tumor that involves killing the malignant cells by subjecting them to extremely high or low temperatures. There are many methods of thermal ablation such as radio-frequency ablation, microwave ablation, and high-intensity ultrasound²⁸. In comparison with traditional surgery, patients that undergo ablation experience much lower rates of long-term side effects including significantly reduced chances of incontinence and a negligible possibility of impotence after surgery²⁹. However, ablation is still a relatively new technique and there are significant opportunities for improvement that may reduce the risks of long-term side effects substantially. The present project focuses primarily on two ablation methods, cryoablation of a tumor which induces cell death by bringing a tumor down to around -40 degrees Celsius a couple of times by freezing and thawing, and laser ablation in which a tumor is exposed to high-intensity laser light resulting in heating of a tumor to 55 °C or higher.

2.2 Cryoablation

Cryoablation is a blanket term referring to the destruction or removal of tissues via freezing. A technique that was first discovered in the mid- 19th century by James Arnott who used salt and crushed ice mixtures to destroy tissue³⁰. Modern cryosurgery has since evolved methods that produce much lower temperatures for targeted cooling of a given tissue, combined with accurate temperature measurement methods. During a cryoablation, surgeons will cool a tumor down to temperatures as low as -50 °C then allow the area to thaw before freezing it again. Each

time the tumor is frozen there is a high chance that the cells within it will die, and by repeating this process a cryosurgery ensures that it kills the malignant tissues³¹.

Cryoablation is performed with a device called a cryo-needle which creates a zone of extremely low temperature around its tip, using thermal properties of gases, specifically adiabatic expansion. A cryo-needle is a system composed of a throttle, which restricts the gas into a closed space; and an expansion chamber, that allows the gas to expand to atmospheric pressure at the tip³². The low temperature at its tip is created by squeezing large volumes of argon through the thin opening inside the hollow needle forcing the gas to its tip where it can briefly expand which, in turn, cools the gas's surroundings, known as the Joules Thompson effect³³. Once the surroundings of the needle have reached the desired temperature the needle is then filled with helium or hydrogen which warm the surroundings as they expand. An effect that occurs due to the unusually weak long range attractive forces in helium and hydrogen gases³⁴.

When a cryoneedle is inserted into a tumor it forms a zone of extremely low temperatures in the flesh that surrounds it creating an 'ice ball', the surface of which is at 0 °C. Though it is worth noting that, 0 °C is not a sufficiently low temperature to kill cancer cells. There are three mechanisms that can cause cell death: rupture of the cell membrane, prolonged dehydration, and local ischemia³¹. If the cooling is slow ice crystals form outside cells drawing water from cells and causing minimal damage repairable through thawing and rehydration of the tissue³⁵. However, if cooling occurs quickly, as induced by the cryoprobe, ice is formed within cells without any dehydration³⁶. By repeating the process of freezing below -20 °C and thawing to room temperature cell membranes are severely damaged, causing their death³⁷. As the malignant cells freeze and thaw, those that don't die are often left in an area the body considers inhospitable, and as an effect

are usually killed off as the body fails to provide the water and blood necessary to reinvigorate them.

The ‘ice ball’ refers to the area where ice formation occurs within the organ. The temperature across the ice ball is not uniform, but is significantly cooler in the center around the cryo-needle³⁸. If the ice ball gets too big then the surgery will likely kill healthy cells along with the cancerous ones but, if the ice ball is too small, the tumor won’t be fully destroyed, and the surgery hasn’t accomplished its main goal³⁹. Thus, monitoring of the temperature within the ‘ice ball’ is an important part of making cryoablation procedures as safe and effective as possible. Ideally, one would like to have accurate three-dimensional temperature maps superimposed on the anatomical image of the tumor throughout the procedure. However, the methods of thermometry currently in clinical use have many flaws that limit the precision with which a surgeon can measure the boundaries of an ice ball and cannot provide an accurate map of the internal temperature.

Methods of temperature mapping in use in operating rooms for cryoablation procedures concern the use of thermocouples, which measure temperature via a voltage change. A thermocouple is composed of two different wires that produce a small voltage when they are heated or cooled at their junction. These devices often have a set temperature range and are limited to measuring temperature at only a single point, thus multiple thermocouples are required to produce even the most rudimentary maps of an organs temperature⁴⁰. To produce the kind of map described previously, one would need to use an unrealistic number of such devices. There exist clear inefficiencies in current thermometry methods. It is clear that, a different method of thermometry that could provide better mapping, would not only be able to speed up many surgeries but also, reduce the potential harm to a patient.

2.3 Laser Ablation

Laser ablation uses intense beams of monochromatic light to destroy cancer cells by heating them typically to temperatures of 55 °C or higher⁴¹. Cells exposed to temperatures between 45 and 55 °C will be irreversibly damaged after prolonged exposure, while cells exposed to temperatures reaching 55 to 60 °C receive damage nearly immediately (a couple of seconds)⁴². This means that surgeries employing laser ablation are dependent on models that predict cell death.

To induce death through overheating, probes are employed, consisting of a laser source powerful enough to heat cells to high enough temperatures to destroy them. To carry the light to deep seated organs, probes also include optical fiber with a diffuser at the end⁴³. Such a probe allows light from a laser to be absorbed by the tissue surrounding the diffuser, creating a heating zone that marks the region where cells have achieved some minimum temperature to destroy them, after some given exposure time⁴⁴. Measuring the extent of this zone can be tricky, since optical probes cannot have thermal couples inserted within them as these might affect the optics of the probe, making the surgery unpredictable. Figure 1 presents the clinical procedure taken from the work of Rastinehad, Ardeshir R., et al. which shows the axial diagram of the surgery alongside an actual image of the trocar needles grouped a laser ablation probe during an ablation procedure⁴⁵. The figure also shows an MRI and ultrasound imaging acquired during surgery, which also highlight the limitations of current imaging methods. Looking closely at the figure it is notable that though the boundaries of the ablation zones are marked no temperature markings are visible. Thermal couples are positioned only to serve as a warning system of damage to the urethra and rectum but are not positioned to give more detailed information about the surrounding healthy tissue. Instead, surgeons must rely on predicted zone expansion from models which can be inaccurate depending on variations in anatomy between individuals.

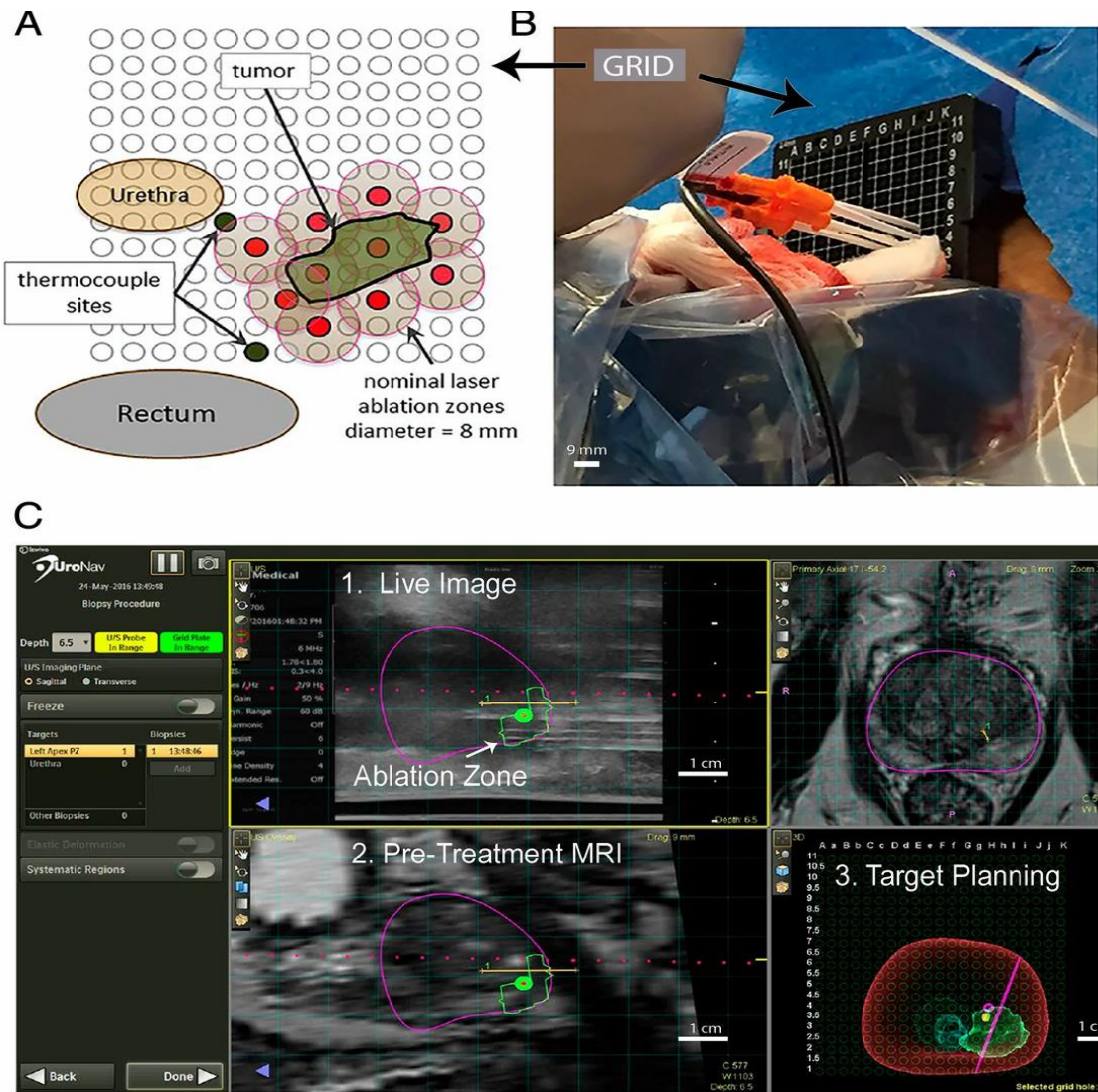


Fig 1. Transperineal approach. **(A)** An axial view of the prostate ablation zone and the nearby urethra and rectum overlaid with a rectangular transperineal grid (3-mm spacing). The ablation zone is penetrated with the introducer trocars (red) through the targeting grid, allowing for the 4- to 5-mm treatment radius(tan). **(B)** Laser introducers (orange hub) placed with the thermocouple (black) through the transperineal grid. **(C)** UroNav MR/US Fusion guidance for trocar placement with real-time ultrasound imaging. 1. Live US and fusion image in which the purple horizontal line is the planned path for the trocars through the virtual target (ablation zone). 2. Pretreatment MRI denoting the prostate (purple), ablation zone region of interest. 3. Targeting screen allows planning for treatment and trocar placement. (Scale bar: B, 9 mm; C, 1 cm.). From 45

2.5 Introduction to Ultrasound

Ultrasound technique employs sound waves of high frequency to detect acoustic boundaries between one medium and another. This is made possible because of the unique properties of sound waves as they travel through mediums. As sound travels, whether it reflects or transmits at boundaries between mediums as well as the speed at which it travels depends on the acoustic properties of the mediums involved. The two most important of these acoustic properties are the acoustic impedance and the stiffness of the material (bulk modulus)⁴⁶.

Stiffness refers to the readiness of a solid to deform from a set shape and is generally represented by the stiffness constant K_s . A larger stiffness constant is representative of a harder material such as a block of iron, while soft materials have small stiffness constants. Sound, like any other kinetic wave, can be thought of as a traveling disturbance of a material being affected by that material's stiffness. If stiffness is the willingness of a material to deform it can also be thought of as the ability of a material to return to its original shape after a small deformation (linear regime)⁴⁷. Stiff materials return to their shape quickly and as a result as traveling sound displaces the plane of atoms forming a disturbance in the material density. This disturbance travels through the material as a sound wave. As stiffness decreases however, atoms take a longer time to return to their equilibrium positions and as such the energy of the sound wave doesn't pass as quickly. Thus, the speed of travel of a sound wave is dependent on the stiffness of a material as well as its density ρ ⁴⁸:

$$v = \sqrt{\frac{K_s}{\rho}} \quad (1)$$

In the common situations in which ultrasound thermometry is applied to study phase transitions, density is often less important to this formula given that the density of a solid tends to change much less with temperature than does its stiffness⁴⁹. As we will discuss below, changes in stiffness can be a very strong function of temperature, a property which will be utilized in our approach to measure temperature within a tissue.

The acoustic impedance of a material refers to how resistant a material is to a sound wave traveling through it. Specifically acoustic impedance Z is defined by⁵⁰:

$$Z = \frac{p}{U} \quad (2)$$

where p is a material's acoustic pressure, the deviation from ambient pressure caused by a sound wave, and U is acoustic volume flow, the volume of particles that are displaced through a plane when a sound wave travels through the medium. Materials with high acoustic impedance require large amounts of energy, to create a kinetic disturbance to travel through⁵¹. In such materials, sound travels slowly. How the acoustic impedances of two materials compare determines how a sound wave will reflect vs. transmit as it tries to travel from one medium to another. If one material requires a significantly different amount of energy for travel as compared to another, then the sound wave will transmit very little into the neighboring medium, preferring instead to reflect back into the medium in which it is currently propagating. This phenomenon is modeled by the reflection, R , and transmission, T , coefficients defined by⁵²:

$$R = \frac{Z_1 - Z_2}{Z_2 + Z_1} \quad (3)$$

$$T = \frac{2Z_1}{Z_1 + Z_2} \quad (4)$$

where Z_1 and Z_2 represent the acoustic impedances of two mediums at their boundary.

Ultrasound works largely due to different structures within the human body having different acoustic impedances⁵³. As sound travels, it eventually hits an area where it is likely to reflect, such as a boundary between a bone and the muscle surrounding it. When the sound hits such a barrier, a portion of it will reflect back to the ultrasound probe while another portion should transmit into the neighboring medium and then reflect off the other side of the object. This phenomenon will result in a series of pulses being measured by the ultrasound probes. From the TOF of a pulse and the relative intensity with which it returns, one can figure out the material the reflector was made of and the distance it is from the probe^{54,55}. When many pulses are sent out the TOF and amplitude can be used to construct a picture that describes the physical structures encountered by the pulses. Modern ultrasound imaging machines also use pulses of varying frequencies that attenuate faster or slower to refine images and distinguish between proximal and more distal objects through which sound has traveled through and bounced off the back side of⁵⁶.

The ability of an ultrasound machine to distinguish between items in a body that are separated is defined through spatial resolution, of which there are two important types; axial and lateral⁵⁷. Axial resolution is the ability of a machine to differentiate between reflectors located parallel to the direction of propagation of the pulse⁵⁸. The value of a pulse's axial resolution is defined as one half of the product between the number of cycles in a pulse and the pulses wavelength λ , more commonly referred to as half the spatial pulse length⁵⁹:

$$\text{Axial Resolution} = \frac{1}{2} * \lambda * (\# \text{ of cycles}) = \frac{1}{2} * (\text{S. P. L}) \quad (5)$$

Lateral resolution refers to the ability of an ultrasound machine to differentiate between reflectors located perpendicular to the axis of propagation of the wave; and is largely dependent on the width

of the pulse beam⁶⁰. This is due to the fact that most ultrasound machines assume that all echoes received at the same time originate from the same object, thus if two separate objects at the same distance from the probe send back a pulse, they are assumed to be the same object⁶¹.

For many ultrasound systems, like those that scan fetuses or check for flaws in a mechanical part, spatial resolution is extremely important; however, in techniques such as ultrasonic thermometry or echocardiography, used for example to show a movie of the working heart, temporal resolution is also very important⁶². Temporal resolution refers to the ability of an ultrasound machine to monitor changes in a system over time⁶³. In general temporal resolution is affected by several factors: speed of propagation of the sound through tissue, depth of field, number of beamlines per field, and the position of the focal point⁶⁴. For the applications explored in this paper, however, only propagation speed and depth of field are relevant as a single piezo component will be employed to generate sound pulses.

To produce data that is precise and accurate enough to create a useful image ultrasound probes are often designed with three principal layers: a piezoelectric layer, a backing layer, and a matching layer; each of which serves an important purpose⁶⁵. The piezoelectric layer is the most important as it is the layer responsible for generation of an ultrasound signal and as such determines the amplitude and frequencies that can be used in the ultrasound machine⁶⁶. The resolution of an ultrasound probe is also determined by this layer, and the frequencies it can generate. This layer is composed of many piezoelectric transducers which mechanically vibrate at a frequency determined by the applied driving ac voltage using the piezoelectric effect⁶⁷. The piezoelectric effect is reversible, it also allows transducers to produce voltages in response to mechanical stress being applied making them both a transmitter and a receiver for an ultrasound machine⁶⁸.

It is for this reason that a backing layer is important for an accurate ultrasound machine, as this layer is responsible for keeping sound from traveling through the piezo more than once⁶⁹. When a piezo vibrates it sends kinetic waves in two primary directions, in front of it as well as behind it. The sound produced behind the piezo electric can bounce off the back of a probe casing and be measured by the piezo, which creates problems in identifying the signal sent through the medium being measured⁷⁰. A backing layer is designed to have a similar acoustic impedance as the piezoelectric itself, and to have a thickness so that back sound produced by the transducer is attenuated away before it can bounce back and be measured by the transducer. This layer also keeps sound sent forward through the medium from being measured by the transducer more than once.

It is often the case that a transducer will have a vastly different acoustic impedance than the medium for which it is trying to measure, which implies a high reflection coefficient at the boundary between the piezo electric layer and the medium⁷¹. To prevent most of the sound being reflected at skin depth, ultrasound probes include a matching layer to create a smooth gradient between the transducer and the medium of interest⁷². This layer is often constructed from epoxies mixed with a variety of metal powders formed into smaller layers of one fourth the wavelength of the signal⁷³. When constructed carefully matching layers can reduce attenuation at the skin boundary by around ninety percent, which improves the chances of a signal being detected greatly⁷⁴. Matching layers also consist of gels placed directly on a patient which improve not only the attenuation cutting effect but also ensure solid contact between the patient and the probe ensuring that no air pockets exist which might create random reflections at the skin boundary⁷⁵.

2.6 Ultrasound Thermometry

In many ways ultrasound thermometry, as envisioned in this paper is a useful and simpler application of the same ideas used in ultrasound imaging. The main difference between using ultrasound to measure temperature versus using it to image a section of a human body comes down to the details of the system through which the sound is traveling. To measure a temperature using ultrasound, the sound must propagate through a system such as a homogeneous block, whose time of flight (TOF), the time that it takes to measure a signal from when it was first sent, can easily be predicted. Using the TOF, velocity can be easily derived using that, t , and the distance the wave traveled through the medium, d , using:

$$v = \frac{d}{t} \quad (6)$$

One can then change the temperature of the block and measure the change in sound velocity resulting from the subsequent change in stiffness. Once this relationship is established, measurements of a pulse's TOF can be directly linked to the temperature of the block using eq. 1.

It is not particularly surprising that using ultrasound thermometry for tumor ablation is not completely a new idea, given that ultrasound is the most popular option for guiding ablation surgeries. However, due to invasive methods of thermometry limiting the benefit of many in-vivo ablation procedures such as high intensity focused ultrasound, little research has been conducted on invasive concepts⁷⁶. Instead, most research in this area concerns strictly non-invasive methods such as Thermal strain, Nakagami imaging, and Tissue Stiffness monitoring^{77,78,79}. For sake of brevity, details of these other methods are included in the literature, as few hold enough current clinical utility to be worth the extensive background they require to explain.

Methods

3.1 Design of an Ultrasound Thermometer

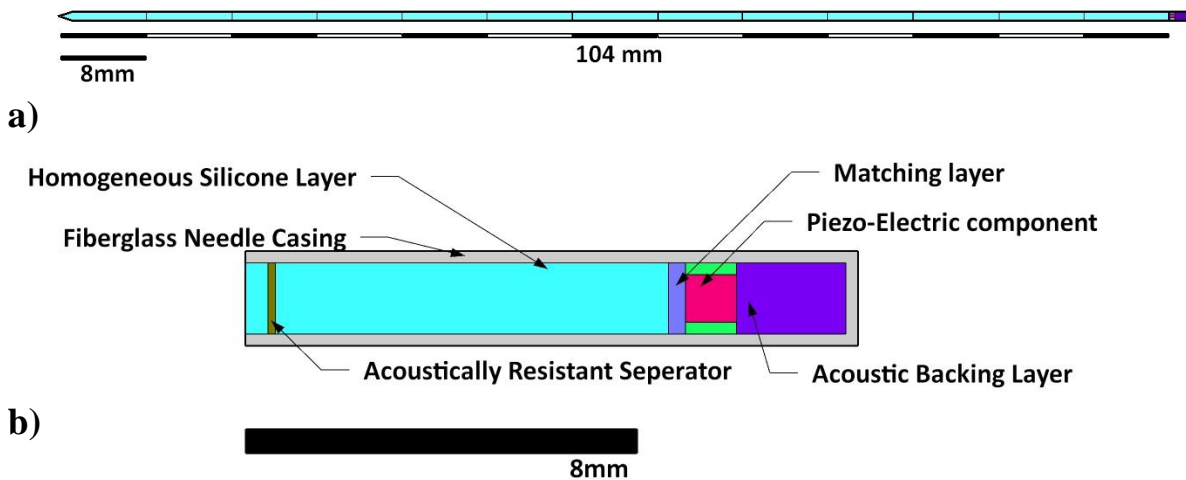


Fig 2. a) a view of a 104 mm probe with 8mm segments separated by small acoustically resistant discs **b)** a close view of the probe segment closest to the piezo-electric transducer

Figure 2 (above) demonstrates the proposed design for an ultrasound thermometry probe, designed to measure temperature as described in section 2.6. The probe consists of several segments of homogeneous silicone, each of 8mm length. Segments are separated by a thin acoustically resistant layer with a strong echogenicity, the ability of a material to bounce an echo. On the back side of the apparatus lies a single piezoelectric transducer with matching and backing layers. It is envisioned that these components could easily fit within a fiberglass needle casing of similar size to the trocar needles already employed in ablation procedures.

Such a probe would be able to make an estimate of the temperature distribution along its main axis by measuring the TOFs of pulses reflecting off the separation layers. The limiting factors of this design are obvious, its resolution is limited to the thickness of a single segment as pulses

are only reflected at separation layers. However, this limitation is not necessarily as significant as it might at first appear, piezo electric components used for ultrasound are of quite high frequency and short wavelength corresponding to a small axial resolution limit. Piezo electric components of small size are common as well, with piezos as small as a 1 mm cube obtainable on even the most meager of budgets. Since most cryo-needles have diameters of around 1.5 mm, this makes it easy to imagine such a setup fitting within the needle. Making the construction of such a device well within the realm of possibility.

Like the currently employed thermal couple methods multiple probes of this type would need to be used to measure around the tumor and completely map the ice ball (Fig 3 ,a). These

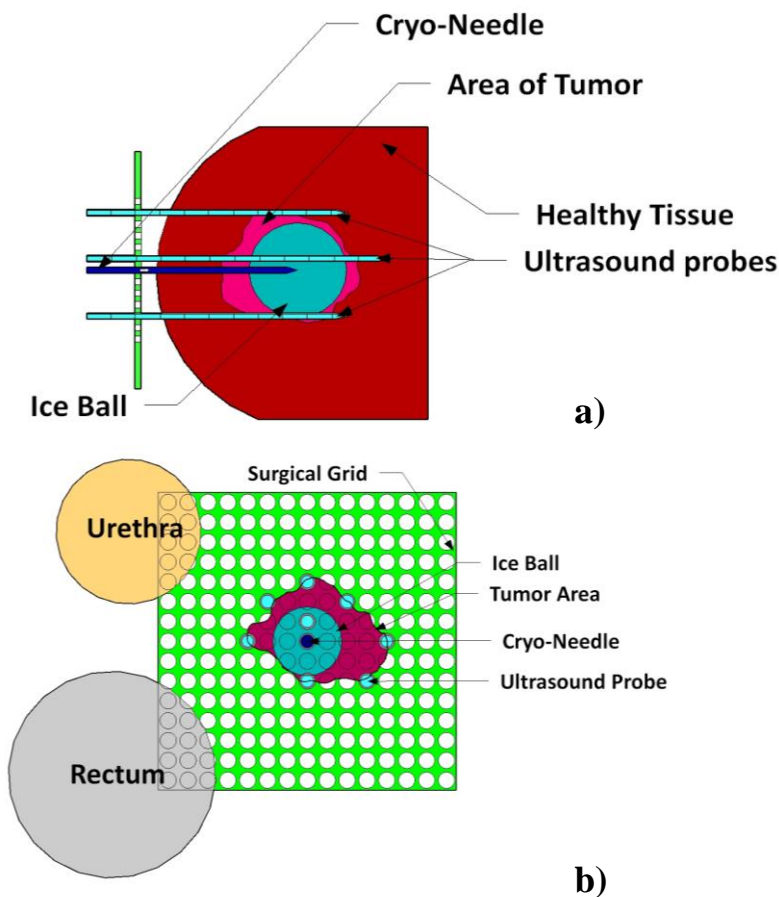


Fig 3. An illustration of how ultrasound probes might be employed in an ablation procedure. **a)** shows placement and depth of probes during surgery with respect to a singular cryo-needle or introduction trocar **b)** Axial view of surgical grid, note the differences from Fig 1a where few thermometry devices are employed despite having several nominal ablation zones

probes would provide a huge advantage over thermal couples, as each probe would be able to measure the temperature profile along its main axis. Such data supplied by only a couple of probes along with the data from the thermocouple at the tip of a cryo-needle, could be used to create a three-dimensional temperature map.

3.2 Setup

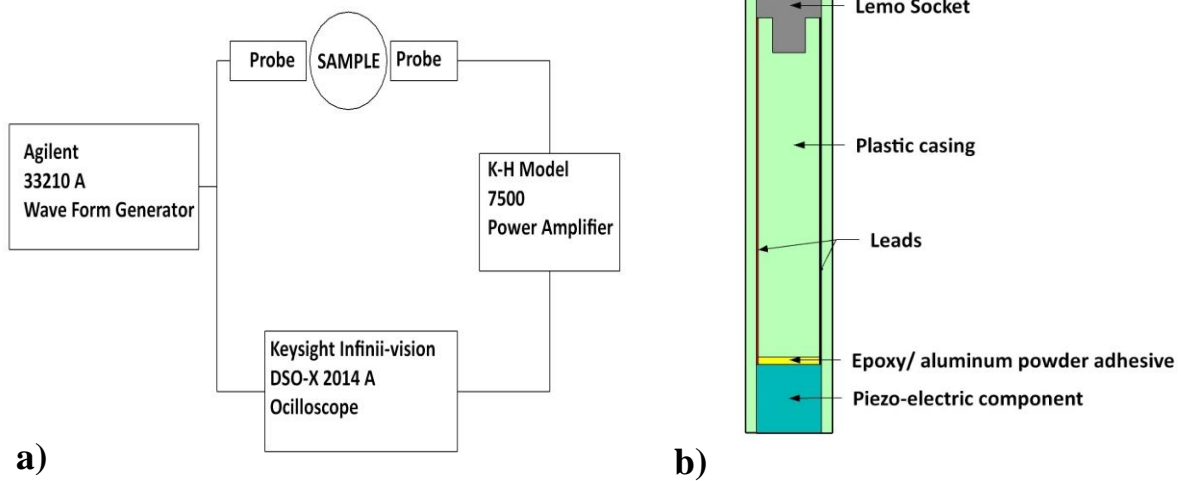


Fig 4. a) Schematic view of the general experimental setup used to obtain temperature curves and measure sound pulses through silicone samples **b)** Schematic of the simple probes constructed for use in homogenous and inhomogeneous sample experiments, these probes and the schematic in a) form what is referred to as the lab made setup in this paper.

Experiments were done to confirm the two most essential aspects of the design described in section 3.1: the temperature dependence of the material to be used in the device, and the ability to see differentiable pulses from corresponding separated segments. In each experiment, a wave form generator was used to create signals at 10Vpp and sent to piezo electric probes that transmitted and measured signals through a polymer sample. Measured signals were then sent through a high voltage amplifier before being passed to an oscilloscope. To make measurement of the TOF easier the scope was triggered using the signal generated from the wave form generator.

The two probes used in these experiments were made in the laboratory so that they could be tailored to the needs of this project. Probes were constructed to provide a proof of concept, and measure trends, more than to provide extremely precise data. Each probe was constructed from a single piezoelectric chip bonded to a polyactic acid plastic case by a thin backing layer consisting of Loctite 9340 Hysol and aluminum nano-powder (Fig. 4b). Matching layers were not included as part of the probe constructions due to the highly difficult and expensive nature of fabricating them. Piezoelectric components used in the probes consisted of a single Thor labs PA1CEW piezoelectric chip with a resonant frequency of 540 kHz and a maximum driving voltage of 45Vpp. In order to limit the interference from backscatter, a backing layer of roughly 1mm was formed out of epoxy and aluminum nano powder.

It is worth noting that to create measurable signals trackable by an oscilloscope these experiments utilized a high voltage, Krohn-Hite Model 7500 wideband power amplifier. Amplifiers such as the one used in these experiments can create large amounts of noise in small amplitude wave forms but allow for signals to be amplified substantially. To prevent the amplifiers clipping signals or being affected by background noise, these circuits were attached to the receiving probe rather than the transmitting probe. This meant that the transmission of ultrasound signals into the sample was smaller than its potential. Nevertheless, these small sound signals were detectable and could be amplified. Another consequence of this choice was that the noise in the signal received by the oscilloscope was comparable to the signal trying to be measured, to counter this several measurements were taken then averaged to sort the random white noise from signal.

Samples of EFX 30 silicone were produced in two different varieties, one in which a plastic separation disc was inserted in the middle before curing and one in which no disc was present. Cylindrical molds were printed using a 3D printer, then sanded to ensure smooth sides to make it

easier to remove samples from the molds. In some samples a delamination solution was used on molds before pouring to assist with removing samples while keeping the molds intact. EFX30 silicone was then mixed in a separate container and poured into the molds. To prevent formation of gas bubbles within the samples, the silicone was degassed after pouring by placing the sample in a vacuum chamber at 15 inHg until no visible bubbles were present. Samples containing a disc were filled halfway, degassed, filled to near full, and degassed again to ensure that gas bubbles would not be present in either half of the sample. Holes roughly one millimeter in diameter were then drilled into samples at several points along their longest side to accommodate thermocouples.

To establish the temperature and its uncertainty in each experiment, thermocouples were used and inserted into samples at semi-regular intervals. Thermocouples were placed such that their tips would lie close to the samples center. In most measurements K-type thermal couples were used, as they have a useful measurement range that easily covers $-50\text{ }^{\circ}\text{C}$ to $50\text{ }^{\circ}\text{C}$, the temperature range of the experiments. It was initially a concern that thermocouples might produce echoes readable by the setup. To put this concern to rest tests were then run to compare the TOF of signals with and without thermocouples. From these tests, it was found that the thermal couples used, produced no reflection capable of interference with data being collected.

3.3 Homogeneous Sample Temperature Experiments

The first experiments conducted focused on determining the correlation between the speed of sound through silicone and its temperature. To do this, a homogeneous silicone sample with four inserted thermal couples, was placed inside an aluminum tube wrapped with thermal heating tape connected to an adjustable power supply. This ensured that the temperature throughout the sample would be homogeneous. The sample was placed between the two ultrasound probes such that the signal from one probe could transmit directly to the other. The sample was then heated

from room temperature up to 50 °C and measurements were taken every 5 °C. At each temperature several measurements were taken at resonant frequency (540 KHz) and 10 Vpp, then averaged to reduce the effect of noise from the amplifier. Similar measurements were then run cooling the sample by surrounding the metal tube in dry ice and cooling it down to -50 °C. Time of flight was then determined at each temperature by taking the averaged data and observing where its first peak lay.

Measurements were then taken at constant temperature using a similar setup. Homogeneous samples were once again placed in a metal tube wrapped in heating tape or surrounded by dry ice. Samples were left to stabilize at a temperature so that many measurements taken at 540Khz could be made with no variance or uncertainty about the exact temperature of the sample. These measurements were then averaged to reduce noise and TOF was determined by measuring the time at which the first peak of the signal appeared. To confirm the frequency of the measured data matched that, of the transmitted signal gradient, a Fourier transform was performed.

3.4 Inhomogeneous Sample Temperature Experiments

To confirm that small separators made of plastic or air could effectively be used as reflectors in a silicone sample, measurements were done on samples where such separators were present. As a proof-of-concept, measurements were done at room temperature using a professionally made defectoscope first, and then confirmed with the lab made setup. As in the homogeneous sample experiments, measurements were taken at constant temperature. Measurements were also taken at changing temperature as well as using a temperature gradient, however, these results are too unrefined at this moment to be included in this paper.

To get clear and easy to decipher results an Olympus 3DL Ultrasonic Thickness Gage was used. Though this device is designed to take measurements of an object's thickness, it works on the same principles as all ultrasound devices and as such, was easy to adapt to this project. The device was used to send ultrasound pulses through several silicone slices separated by air. The results on the devices screen were then recorded and compared to the measured thicknesses of the slices in order to determine if the separations were indeed acting as reflectors. Due to the limited penetration depth of the thickness gage experiments on samples with plastic reflectors inserted were unable to be performed using this device. Instead, experiments were run using the lab made setup, to confirm that the results from the commercial device were relevant to those in the sample experiments.

The experiments using the lab built set up were carried out in the following manner. Samples were placed on a table with both probes situated on the top face. A pulse was then sent and recorded by an oscilloscope via the same setup used in the experiments on the samples with no reflector present. The same method of averaging and frequency checking was performed. The time of flight in the first section was then determined by measuring the first observable peak. The time of flight for the second section was determined by identifying the end of the first wave pattern and measuring the first peak of the second wave pulse.

3.5 Probe Modeling

Using the TOF data collected from the experiments mentioned above, velocity was then determined using eq. 6. These velocities were then associated with the temperatures of the samples and curves were produced to model the speed of sound as a function of temperature. Due to the averaging techniques used in the collection of this data errors in both temperature and velocity were calculated to ensure that predictions were accurate. These results were then used to model

the behavior of a theoretical probe consisting of several homogenous layers of silicone as described previously. Layers were modeled to be 8 mm long with a variance of +/- 0.01 mm to simulate the imprecision often present in silicone pouring. The modeled probe was simulated to have 13 segments making it 10.4 cm long, a common size for trocar needle. Several simulations were run to model different temperature distributions ranging from non-physical results to more realistic cases. In each case, the temperature dependence relation of velocity in silicone was used to predict the temperature distribution in the modeled probe.

A probe was modeled filled with segments of EFX30 silicone, by means of the temperature-velocity relations mentioned previously. It was assumed that attenuation throughout the probe, which is strongly dependent on acoustic impedance of a material, was ignorable. It was also assumed that pulses were reflected and transmitted perfectly. In other words, it was assumed that this probe was ideal in that reflections off separation layers would always be measurable. Though attenuation properties are important considerations in the design of a probe such as the one described in this paper. Modeling these attributes requires knowledge of the acoustic impedance of the materials used in the probe's construction to a reasonable degree, which was not possible given the limitations of the equipment available.

Using these assumptions, several models were produced to demonstrate the theoretical qualities of the probe design. The first case (Fig. 5a) was that of a probe with each section maintaining a constant temperature that varies between segments, with a minimum temperature at the center of the probe. Other physical examples were explored, such as a similar kind of distribution with an asymmetric shape, which might occur along a cryo-needle where temperature is cold only around the tip (Fig. 5b). Though discontinuous cases such as these are not found in

the physical world, their inclusion helps guide understanding of the exact quantities the probe measures.

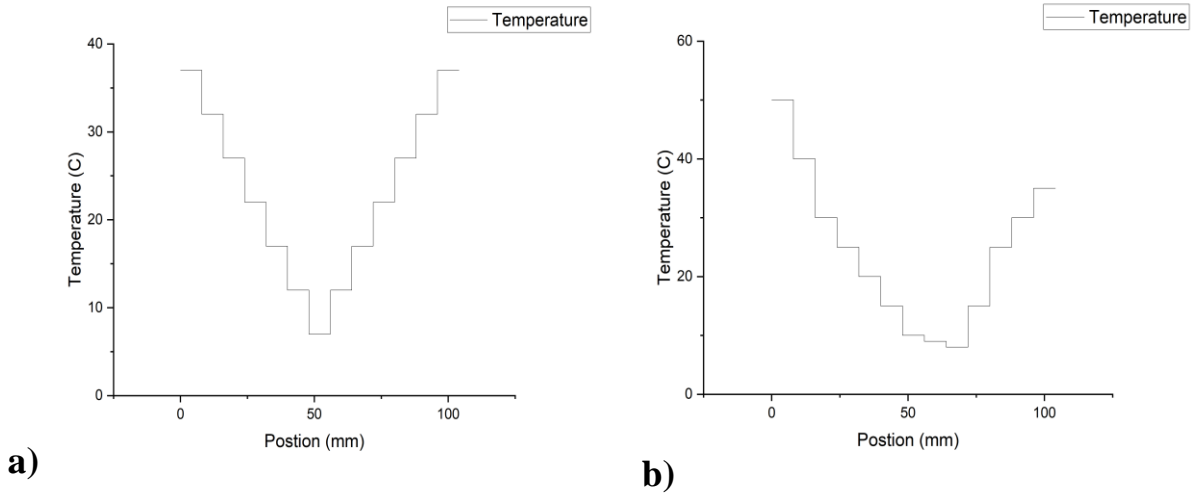


Fig 5. a) graph of non-continuous symmetric temperature model used in the probe modeling calculations **b)** graph of non-continuous asymmetric temperature model used in probe modeling

Continuous cases were also considered, as these bear more resemblance to reality. First two symmetric cases were studied, a linear v-like temperature distribution (7) and a parabola (8):

$$T(x) = 500 * |x * 0.001 - 0.056| + 7 \quad (7)$$

$$T(x) = 13020.834 * (x - 0.056)^2 + 7 \quad (8)$$

where $T(x)$ is the temperature expressed as a function of distance from the probe head. Each of which, modeled a more realistic case of the distribution shown in Fig. 5a. An asymmetric distribution was also modeled using a Chi-squared distribution:

$$T(x) = 37 - 1000 * e^{\frac{-500 * ((104-x) * 0.001)}{13}} \sqrt{\frac{5}{13 * \pi}} * \sqrt{(104 - x) * 0.001} \quad (9)$$

which models a continuous case of an asymmetric distribution, like the one depicted in Fig 5b. TOF was then determined by plugging these continuous temperature distributions into the temperature vs. wave velocity curve, a linear function obtained from the homogeneous sample experiments, producing a spatial speed distribution., then integrating over one probe segment (8mm):

$$TOF = 2 * \int_{d-0.008}^d \frac{1}{a*T(x)+b} dx \quad (10)$$

Results & Discussion

4.1 Discussion of Homogenous Sample Results

Experiments run on homogeneous samples produced many pulse measurements that show clear sound propagation through the samples. Pulse profiles produced showed several extra peaks than were supplied from the signal generator implying either back noise or an electrical resistance mismatch. However, these artifacts did not have any conceivable effect on measurement of TOF

which relies only on the first peak's occurrence. From viewing the collected profiles (Fig 6), movement in the first peak of the signal is clearly visible between measurements collected at varying temperatures. These profiles also highlight the ambiguity present in determining TOF even

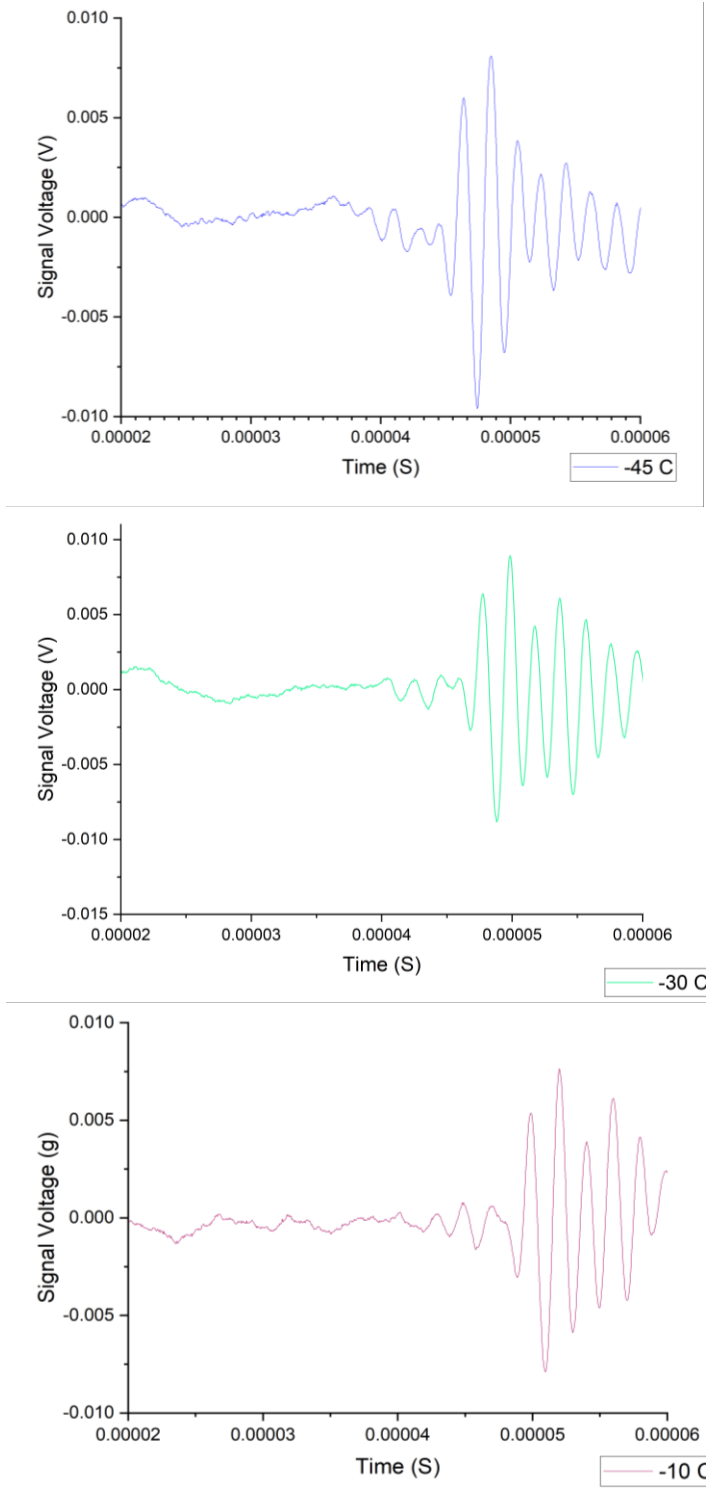


Fig 6. Shows pulse signals measured at -45 °C, -30 °C, -10 °C respectively, not how points where periodic behavior begins is slowest at -10 °C and fastest for -45 °C

as most of the noise has been averaged away. While there exists a point at which a periodic signal is clearly dominating in all these profiles, the point at which the signal is actually received is not as clear, as one might hope. This stresses the need to use a Fourier transform to assist proper determination of the first signal peak in each case.

Once TOF was confidently determined, the velocities were plotted as a function of temperature. The experimental data points were then fitted to a line. However, many iterations of these experiments produced fitted lines with notable variance. This was likely due to compression of the sample by the probes resulting in uncertainty in the distance traveled by the wave. To remedy this, points from multiple identical experiments were taken and averaged to produce a curve less subject to this uncertainty, Fig 7. These curves were repeated at temperatures ranging from room temperature to 50 °C.

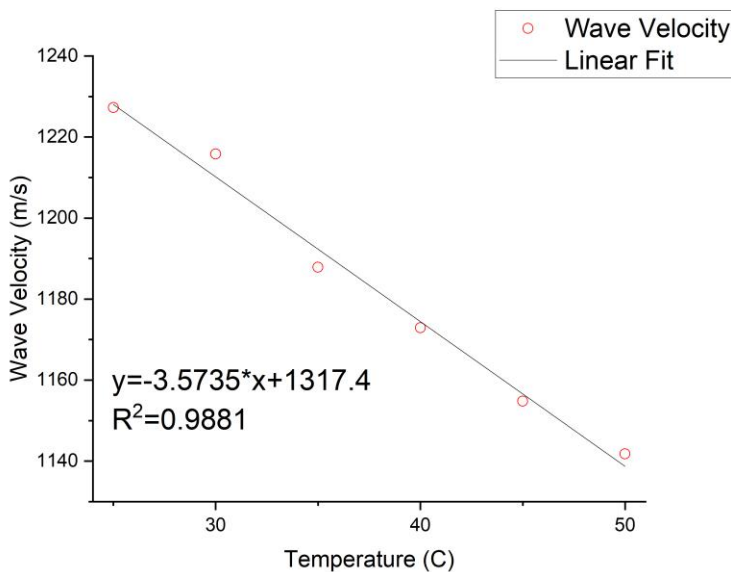


Fig 7. Averaged linear fit from temperature change experiments. Fits produced from multiple experiments produced graphs with consistent slopes but varying y-intercepts, thus the results of four different iterations of an identical experiment were averaged to produce a fit. Note errors were not included as the number of points averaged produced an error too small to be seen on this graph.

The linear fit shown in Fig 7, demonstrates a strong temperature dependence for the speed of sound through silicone from room temperature (~22 °C) to 50 °C. It is worth noting that, measurements taken in other experiments also suggest that this relation remains similarly linear

all the way down to $-50\text{ }^{\circ}\text{C}$, giving strong evidence that such silicones would be useful thermometry choices for both cryoablation and laser ablation. However, at the current moment not enough reliable data was produced to confidently extend these results to temperatures down to $-50\text{ }^{\circ}\text{C}$. This being said, the similarity between the curves taken across $-50\text{ }^{\circ}\text{C}$ to room temperature and those shown in Fig. 7 show strong evidence in support of such silicones being useful thermometry choices not only in laser ablation but also in cryoablation as well. The preliminary data produced from these experiments also show a reliable slope that doesn't vary significantly between multiple iterations (data not shown). This preliminary data also gives a moderately detailed picture of the temperature dependence that these materials offer in the range of -50 to $50\text{ }^{\circ}\text{C}$. Namely, that within this range EFX 30 doesn't freeze, causing a sharp spike in its stiffness and subsequently in the speed of sound through the medium in this range of temperatures. Such a phase transition, would result in inaccurate and difficult to decipher data in an ultrasound thermometry probe.

Table 1. Experimental velocities calculated using measured times of flight taken as the sample was held at constant temperature compared to predicted velocities calculated using linear fit model produced from the homogeneous sample experiments.

Measured Temperature (C^o)	Calculated Velocity ($\frac{m}{s}$) (from time of flight measurement)	Predicted Velocity ($\frac{m}{s}$) (from linear fit)	% Velocity error	Predicted Temperature (C^o) (from linear fit)	% Temp. error
22	1235.955	1238.783	0.2288	22.79	3.597
33	1205.1	1199.4	0.4668	31.43	4.77
38.7	1180.3	1179.1	0.1012	38.37	0.8637
47.6	1158.537	1147.3	0.9698	44.46	6.605

Also notable, is the agreement between the constant temperature measurements and the predictions given by Table 1. Despite the ambiguity and uncertainty in the setup, the predictions made for both velocity and subsequently for temperature are relatively low. The percent error between the predicted and measured velocities is very small, under 1% for all temperatures. Though there is significantly more error in the predicted temperature values, these are not unexpected given the lack of tuning in the ultrasound probes used. Suggesting that the concept is strong enough to produce accurate results, even using rudimentary probes like the ones constructed for this experiment. Though there is clearly room for improvement before any clinical usage could be considered.

4.2 Discussion of Inhomogeneous Sample Results

Using the Olympus thickness gauge measurements were taken that show multiple pulses being visibly measured from a sample (Fig. 8). The sample used was composed of several homogeneous slices of EFX 30 silicone separated by thin layers of air. As the figure shows, three pulses were observed on the thickness gauge's display at distances corresponding to 6, 13, and 28 mm. This shows that accurate measurements are able to be made using discs of a silicone separated by air or plastic. When combined with the data collected from the temperature dependence tests, this provides a strong indication that an ultrasound device designed as described could provide a reliable method for temperature measurement.

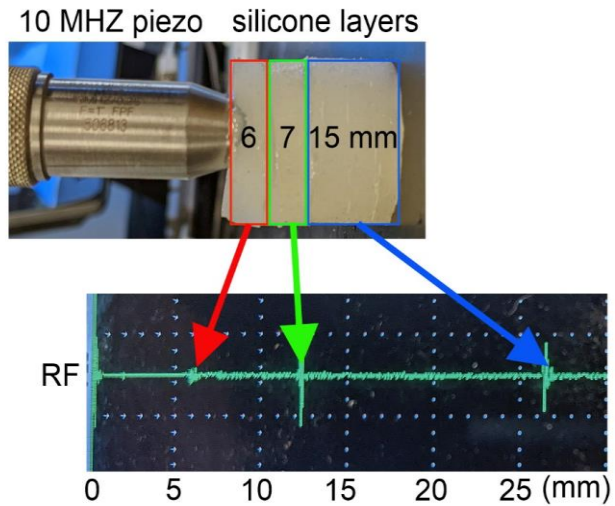


Fig 8. A picture of a proof of concept experiment performed with an ultrasonic thickness gage using a sample composed of 6mm, 7mm, 15mm. Showing three separate pulses corresponding to the location of the separate pulses corresponding to the location of the reflector between consecutive segments.

Measurements were also done to demonstrate this same principle with thicker samples using the lab constructed probe setup. Though multiple measurements were done this way, peaking artifacts as discussed in section 4.1 tended to blur the separate pulses from the disc, and the back of the sample together, making them hard to distinguish except at high temperatures where the pulses traveled slower. In this data two clear packets appear representing the pulse bouncing off the disc and the subsequent bounce off the bottom of the sample. Which provides further evidence that not only can these separations be visible but are clear even at longer distances.

The data collected from these experiments provides solid evidence that the silicone used does not only show strong temperature dependent stiffness but that small separations of this medium produce pulses distinguishable even in extremely prototypical probes. It seems evident then that such a probe, presents a promising method for ultrasound imaging in ablation surgeries. Several sections composed as described earlier in this paper would produce pulses whose distance from one another could be used to determine the temperature of each section.

4.3 Discussion of Probe Modeling

Probes were modeled using the linear temperature dependence fit obtained from the homogeneous sample measurements applied to simulated temperature distributions. For non-continuous cases temperatures were plugged into the fit equation to predict the velocity of sound through segments of that temperature. Twice the length of the segment was divided by this velocity to obtain the TOF of the signal reflected at the boundary. Figure 9 shows the differences in these times of flight, e.g. the time difference between the pulses as plotted against position; note that these graphs also include a temperature scale on their right axis.

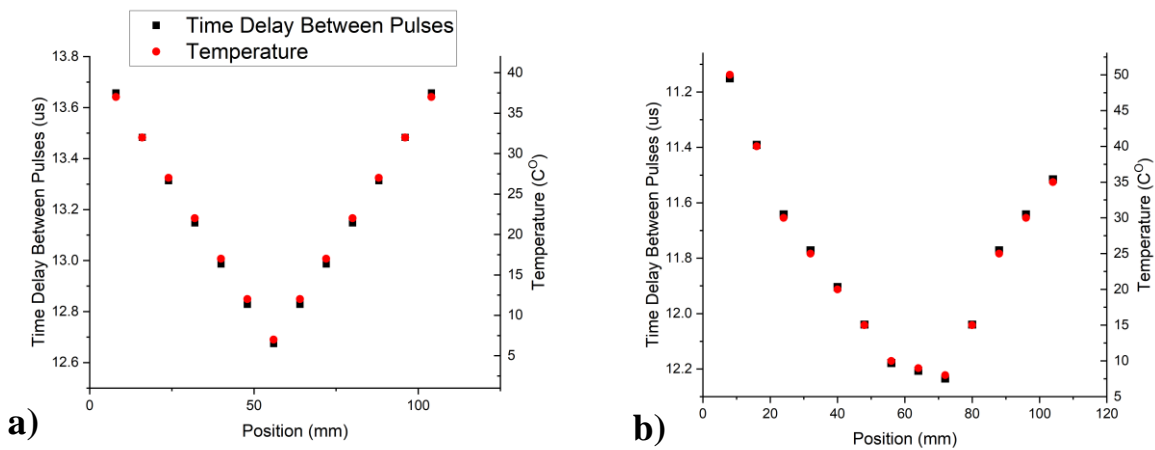


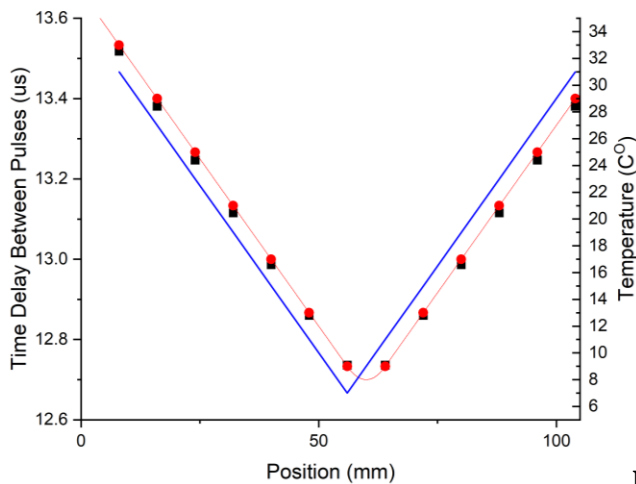
Fig 9. Graphs comparing the temperature at point of reflection to time delay between consecutive pulses for the non-continuous temperature distributions described in 3.5 **a)** a symmetric distribution with temperatures ranging from 7 °C to 37 °C. **b)** an asymmetric distribution with temperatures ranging from 8 °C to 50 °C

Through these graphs it is easy to see how well a theoretical probe and the delays of pulses received can be used to model the temperature of a segment. The points of an average temperature vs. position graph, and a time delay between pulses vs. position graph can be almost perfectly imposed upon one another (Fig 9). This allows for easy matching between delay time and temperature.

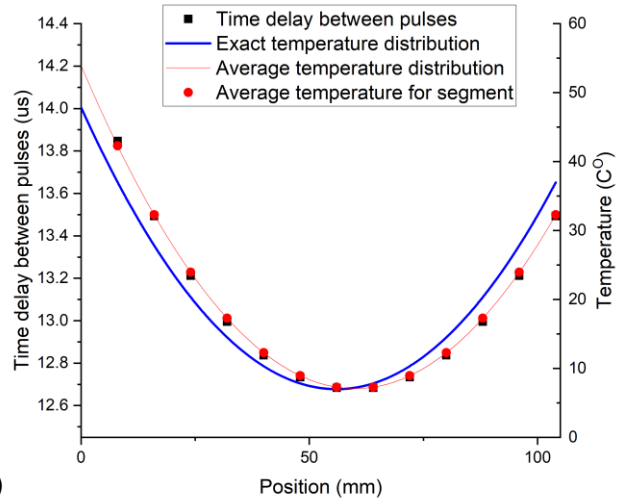
For continuous temperature distributions, temperature dependent changes in velocity were determined as a function of position using the same relations used in the non-continuous models. An integral was then taken as shown (eq. 10, section 3.5) to produce the TOF curves shown in Fig. 10. These were then compared to a curve composed of average temperature values found by taking the integral of the exact temperature distribution as shown:

$$\textit{Average temp}(x) = \frac{\int_{d-0.008}^d T(x)}{8*0.001} \quad (11)$$

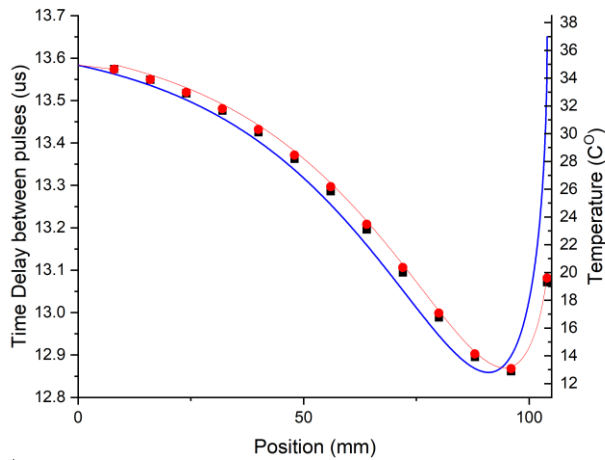
where d is the distance along the probe, and T(x) is the exact temperature distribution function.



a)



b)



c)

Fig 10. Set of graphs comparing the exact and average temperature distributions to the modeled TOFs using the methods described in 3.5 **a)** graph of the linear v-like symmetric continuous distribution modeled by the temperature distribution eq. 7 **b)** graph of the parabolic symmetric temperature distribution modeled by eq. 8 **c)** graph of the asymmetric chi-squared distribution with temperatures ranging from ~ 13 °C to ~ 34 °C

Though, results show a clear offset from the exact temperature distribution the similarity to the average temperature curves is worth remark. One can observe that the time delay points follow the temperature average for each section better than they follow the points of the exact distribution. This is to be expected as the time for sound to travel through a section of the probe is dependent on the temperature distribution of that section and not the temperature at the point of reflection. This result also stresses the importance of the piezo used, as this part also effects the axial resolution of the probe and thus, how small or large each section needs to be to produce

differentiable pulses. The smaller each section can become the more information the probe will be able to gather, but this also brings the risk of separate pulses not being clearly identifiable.

Conclusion

Thermal ablation is a surgical method currently in clinical development, that destroys tissue through subjecting it to extreme temperatures. Though there are many limitations to this kind of surgery, it holds many advantages over the current medical standard treatments like radiation and traditional surgery. Many of the issues for thermal ablation are due to the limited modes of temperature measurement currently in use in operating rooms. Existing thermometry methods are limited to the use of thermocouples that can only measure temperature at a single point. This makes three-dimensional mapping difficult without employing many thermocouples, which can impede a surgeon.

This project explored the viability for an ultrasound probe design to replace the current methods of thermometry in use in thermal ablation procedures. The design presented in this paper consisted of a fiberglass needle of similar size to the trocar needles already in use in the operating room, filled with segments of silicone separated by reflecting layers. Rather than using voltage, the described probe uses the temperature dependent, mechanical properties of a silicone medium to make an estimate of temperature using the TOF of a sound wave. Such a design promises to improve upon current methods of thermometry by providing the capability to take real-time three dimensional temperature maps of a tumor during a procedure.

To test the viability of such a probe, experiments were performed to test the two most basic attributes of the design: the temperature dependence of sound's velocity through the medium and the echogenicity of thin separation layers. To test temperature dependence, ultrasound probes were designed and used to measure the TOF of ultrasound layers through silicone samples at a variety

of temperatures. Results were then compiled and used to create linear fits relating the velocity as calculated from TOF to the samples temperature. Predictions from these fits were then compared to measured results taken at constant temperature. Despite the use of rudimentary equipment, results supported the use of a silicone like material in measuring temperature with surprising accuracy. Though issues remain with artifacts present in many measurements.

To test echogenicity, samples were prepared that included reflectors and ultrasound pulses were run through them. Echogenicity measurements were also run using a professionally made probe to ensure that results collected could be relied upon. From these tests it was confirmed that thin reflectors would be able to produce pulses of significant enough amplitude to register with a piezoelectric probe. Combined with the results of temperature dependence experiments, these results set a strong case for the utility of such a design being feasible.

Using results from the experiments described, models were then developed to predict the theoretical behavior of a probe. To do this multiple temperature distributions were explored ranging from purely theoretical to physically possible. As predicted models showed strong dependence of TOF with temperature. As expected, calculated values trended with a section's average temperature rather than exact temperature. The results from the probe modeling showed implications for the resolutions of such a probe, namely that it is limited to the length of a single segment and number of segments in the probe.

Future Work

The results described in this paper are representative of a proof-of-concept for the probe design described. As such, there is a lot of work that remains to be done in the development and refinement of these probes, and many questions remain unsolved. Work must be done in improving the accuracy of the probes, as the results of this paper are enough to support temperature

dependence but are a long way off from being ready for clinical use where lives are at stake. Results presented in this paper must also be explored in temperature ranges exceeding 50 °C to ensure that they are indeed valid for the temperature ranges used in laser ablation (up to 70 °C). Experiments must also be done to more accurately measure the results down to -50 °C to ensure that the monotonic relation discussed is indeed accurate and usable in cryoablation.

Further, many aspects of the probes design remain unfulfilled, though ultrasound probes often come in sizes that can fit within a trocar needle, there may still be several issues with probe construction. Namely, matching the size of the component to the frequencies necessary to make useful thermometer measurements for an ablation, may still prove difficult. Though this paper has explored the capacity of sound waves to travel long distances of up to 60mm this is still half of the simulated length in the models. Thus, experiments must be done to ensure that a signal will not attenuate through such a long probe.

The resolution of such a probe also remains largely unexplored. Even if sound can travel through a probe of nearly twice the length as was tested in this paper, the number of segments will also influence the attenuation. Thus, exploration must be done to find a ‘goldilocks ratio’ of sorts between the probe’s resolution and the attenuation from the reflecting layers. Temporal resolution of the probe must also be explored. Though the theoretical temporal resolution limit of the probe is indeed limited to the time it takes for the pulse to travel to the needle’s tip and back many methods could be used to improve this. A piezoelectric can produce many frequencies and could theoretically send pulses of several frequencies and sort them using Fourier transform. Such methods could make the probe even more accurate and produce to real-time measurements.

Thus, much work remains before a probe could even be considered for clinical trials, though evidence suggests that the concept at least is sound. It is for this reason that the group’s

main goals are to apply for funding and patent the design concept so that more in depth exploration can be done.

Bibliography

1. Han, Xuesong, et al. "Medical Financial Hardship Intensity and Financial Sacrifice Associated with Cancer in the United States." *Cancer Epidemiology Biomarkers & Prevention*, vol. 29, no. 2, 2020, pp. 308–317.,
<https://doi.org/10.1158/1055-9965.epi-19-0460>.
2. Siegel, Rebecca L., et al. "Cancer Statistics, 2022." *CA: A Cancer Journal for Clinicians*, vol. 72, no. 1, 12 Jan. 2022, pp. 7–33.,
<https://doi.org/10.3322/caac.21708>.
3. Surveillance, Epidemiology, and End Results (SEER) Program (www.seer.cancer.gov) SEER*Stat Database: Mortality - All COD, Aggregated With State, Total U.S. (1969-2018) <Katrina/Rita Population Adjustment>, National Cancer Institute, DCCPS, Surveillance Research Program, released May 2020. Underlying mortality data provided by NCHS (www.cdc.gov/nchs).
4. Warren, J. L., et al. "Evaluation of Trends in the Cost of Initial Cancer Treatment." *JNCI Journal of the National Cancer Institute*, vol. 100, no. 12, 2008, pp. 888–897.,
<https://doi.org/10.1093/jnci/djn175>.
5. Evans, D Gareth, et al. "Improvement in Risk Prediction, Early Detection and Prevention of Breast Cancer in the NHS Breast Screening Programme and Family History Clinics: A Dual Cohort Study." *Programme Grants for Applied Research*, vol. 4, no. 11, 26 Aug. 2016, pp. 1–210.,
<https://doi.org/10.3310/pgfar04110>.
6. Konoshenko, Maria Yu., et al. "The Panel of 12 Cell-Free MicroRNAs as Potential Biomarkers in Prostate Neoplasms." *Diagnostics*, vol. 10, no. 1, 2020, p. 38.,
<https://doi.org/10.3390/diagnostics10010038>.
7. American Cancer Society. *Cancer Treatment & Survivorship Facts & Figures 2019-2021*. Atlanta: American Cancer Society; 2019.
8. Tohme, Samer, et al. "Surgery for Cancer: A Trigger for Metastases." *Cancer Research*, vol. 77, no. 7, 2017, pp. 1548–1552.,
<https://doi.org/10.1158/0008-5472.can-16-1536>.
9. Yılmaz, Saim, et al. "Use of Cryoablation beyond the Prostate." *Insights into Imaging*, vol. 7, no. 2, 2016, pp. 223–232.,
<https://doi.org/10.1007/s13244-015-0460-7>.
10. Brace, Chris. "Thermal Tumor Ablation in Clinical Use." *IEEE Pulse*, vol. 2, no. 5, 2011, pp. 28–38.,
<https://doi.org/10.1109/mpul.2011.942603>.
11. Zhou, Yanzhao, et al. "Challenges Facing Percutaneous Ablation in the Treatment of Hepatocellular Carcinoma: Extension of Ablation Criteria." *Journal of Hepatocellular Carcinoma*, Volume 8, 21 June 2021, pp. 625–644.,
<https://doi.org/10.2147/jhc.s298709>.
12. Agyekum, Enock Adjei, et al. "Ultrasound-Guided Thermal Ablation of Thyroid Nodules: Technicalities Progress and Clinical Applications, Especially in Malignant Thyroid Nodules." *Frontiers in Oncology*, vol. 11, 2021,
<https://doi.org/10.3389/fonc.2021.761005>.
13. Baust, John, et al. "Minimally Invasive Cryosurgery—Technological Advances." *Cryobiology*, vol. 34, no. 4, 1 Oct. 1997, pp. 373–384.,
<https://doi.org/10.1006/cryo.1997.2017>.
14. Hankiewicz, Janusz H., et al. "Measurement of Sub-Zero Temperatures in MRI Using t_1 Temperature Sensitive Soft Silicone Materials: Applications for MRI-Guided Cryosurgery." *Medical Physics*, vol. 48,

- no. 11, 2021, pp. 6844–6858.,
<https://doi.org/10.1002/mp.15252>.
15. Woodrum, David A., et al. “Magnetic Resonance–Guided Prostate Ablation.” *Seminars in Interventional Radiology*, vol. 36, no. 05, 2019, pp. 351–366.,
<https://doi.org/10.1055/s-0039-1697001>.
 16. Cheng, Zhigang, and Ping Liang. “Advances in Ultrasound-Guided Thermal Ablation for Symptomatic Benign Thyroid Nodules.” *Advances in Clinical and Experimental Medicine*, vol. 29, no. 9, 2020, pp. 1123–1129.,
<https://doi.org/10.17219/acem/125433>.
 17. Assorted. “Compression Waves.” *Compression Waves - an Overview | ScienceDirect Topics*, Elsevier,
<https://www.sciencedirect.com/topics/physics-and-astronomy/compression-waves>.
 18. Ball, John, et al. *Ball and Moore's Essential Physics for Radiographers*. Blackwell Science, 2008.
 19. Chen, Fang-zhi, and Xiao-kun Zhao. “Prostate Cancer: Current Treatment and Prevention Strategies.” *Iranian Red Crescent Medical Journal*, vol. 15, no. 4, 2013, pp. 279–284.,
<https://doi.org/10.5812/ircmj.6499>.
 20. Siegel, Rebecca L., et al. “Cancer Statistics, 2021.” *CA: A Cancer Journal for Clinicians*, vol. 71, no. 1, 2021, pp. 7–33.,
<https://doi.org/10.3322/caac.21654>.
 21. Trogdon, Justin G., et al. “Total Medicare Costs Associated with Diagnosis and Treatment of Prostate Cancer in Elderly Men.” *JAMA Oncology*, vol. 5, no. 1, 2019, p. 60.,
[doi:10.1001/jamaoncol.2018.3701](https://doi.org/10.1001/jamaoncol.2018.3701).
 22. Assorted. “Prostate Cancer.” *Mayo Clinic*, Mayo Foundation for Medical Education and Research, 4 June 2021,
<https://www.mayoclinic.org/diseases-conditions/prostate-cancer/diagnosis-treatment/drc-20353093>.
 23. “What to Expect When Having Radiation Therapy.” *Cancer.Net*, American Society of Clinical Oncology, 23 Sept. 2020,
<https://www.cancer.net/navigating-cancer-care/how-cancer-treated/radiation-therapy/what-expect-when-having-radiation-therapy#:~:text=Typically%2C%20people%20have%20treatment%20sessions,healthy%20tissue%20surrounding%20the%20tumor>.
 24. “Radiation Therapy Side Effects.” *National Cancer Institute*, 11 Jan. 2022,
<https://www.cancer.gov/about-cancer/treatment/types/radiation-therapy/side-effects>.
 25. Takahashi, Takeo, et al. “Evaluation of Quality of Life and Psychological Response in Cancer Patients Treated with Radiotherapy.” *Radiation Medicine*, vol. 26, no. 7, 4 Sept. 2008, pp. 396–401.,
<https://doi.org/10.1007/s11604-008-0248-5>.
 26. McCullough, Andrew R. “Sexual Dysfunction after Radical Prostatectomy and the Use of Pde-5 Inhibitors.” *Oral Pharmacotherapy for Male Sexual Dysfunction*, 2005, pp. 409–421.,
[doi:10.1385/1-59259-871-4:409](https://doi.org/10.1385/1-59259-871-4:409).
 27. Stanford, Janet L., et al. “Urinary and Sexual Function after Radical Prostatectomy for Clinically Localized Prostate Cancer.” *JAMA*, vol. 283, no. 3, 19 Jan. 2000, p. 354.,
[doi:10.1001/jama.283.3.354](https://doi.org/10.1001/jama.283.3.354).
 28. “About Your Prostate Ablation Procedure.” *Memorial Sloan Kettering Cancer Center*, 1 Jan. 1970,
<https://www.mskcc.org/cancer-care/patient-education/about-prostate-ablation-procedure#:~:text=Prostate%20ablation%20is%20a%20procedure,the%20surrounding%20normal%20prostate%20tissue>.
 29. “Cryotherapy for Prostate Cancer.” *American Cancer Society*, American Cancer Society, 1 Aug. 2019,
www.cancer.org/cancer/prostate-cancer/treating/cryosurgery.html.
 30. Cooper, S M, and R P Dawber. “The History of Cryosurgery.” *Journal of the Royal Society of Medicine*, vol. 94, no. 4, Apr. 2001, pp. 196–201.,

- <https://doi.org/10.1177/014107680109400416>.
31. Gage, Andrew A., and John Baust. "Mechanisms of Tissue Injury in Cryosurgery." *Cryobiology*, vol. 37, no. 3, 21 July 1998, pp. 171–186., <https://doi.org/10.1006/cryo.1998.2115>
 32. Erinjeri, Joseph P., and Timothy W.I. Clark. "Cryoablation: Mechanism of Action and Devices." *Journal of Vascular and Interventional Radiology*, vol. 21, no. 8, 21 Aug. 2010, <https://doi.org/10.1016/j.jvir.2009.12.403>.
 33. Britannica, The Editors of Encyclopaedia. "Joule-Thomson effect". *Encyclopedia Britannica*, 21 Apr. 2017, <https://www.britannica.com/science/Joule-Thomson-effect>. Accessed 29 March 2022.
 34. Ozerov, Ruslan P., and Anatoli A. Vorobyev. "Molecular Physics." *Physics for Chemists*, 19 Oct. 2007, pp. 169–250., <https://doi.org/10.1016/b978-044452830-8/50005-2>.
 35. Baust, J.G., et al. "Mechanisms of Cryoablation: Clinical Consequences on Malignant Tumors." *Cryobiology*, vol. 68, no. 1, 13 Nov. 2013, pp. 1–11., <https://doi.org/10.1016/j.cryobiol.2013.11.001>.
 36. Mazur, Peter, et al. "Kinetics of Water Loss and the Likelihood of Intracellular Freezing in Mouse OVA." *Cell Biophysics*, vol. 6, no. 3, 18 June 1984, pp. 197–213., <https://doi.org/10.1007/bf02788619>.
 37. Cooper, Irying S. "Cryobiology as Viewed by the Surgeon." *Cryobiology*, vol. 1, no. 1, 1964, pp. 44–51., [https://doi.org/10.1016/0011-2240\(64\)90019-7](https://doi.org/10.1016/0011-2240(64)90019-7).
 38. Yamashita, Masanori, et al. "Evaluation of Temperature Distribution around the Probe in Cryoablation of Lipiodol-Mixed-Tissue Phantom." *CardioVascular and Interventional Radiology*, vol. 44, no. 3, 2020, pp. 489–495., <https://doi.org/10.1007/s00270-020-02710-3>.
 39. Su, Wilber, et al. "Best Practice Guide for Cryoballoon Ablation in Atrial Fibrillation: The Compilation Experience of More than 3000 Procedures." *Heart Rhythm*, vol. 12, no. 7, 2015, pp. 1658–1666., <https://doi.org/10.1016/j.hrthm.2015.03.021>.
 40. Myers, Donna N. "Innovations in Monitoring with Water-Quality Sensors with Case Studies on Floods, Hurricanes, and Harmful Algal Blooms." *Separation Science and Technology*, 23 May 2019, pp. 219–283., <https://doi.org/10.1016/b978-0-12-815730-5.00010-7>.
 41. Schena, Emiliano, et al. "Laser Ablation for Cancer: Past, Present and Future." *Journal of Functional Biomaterials*, vol. 8, no. 2, 2017, p. 19., <https://doi.org/10.3390/jfb8020019>.
 42. Sapareto, Stephen A., and William C. Dewey. "Thermal Dose Determination in Cancer Therapy." *International Journal of Radiation Oncology*Biophysics*Physics*, vol. 10, no. 6, 10 June 1984, pp. 787–800., [https://doi.org/10.1016/0360-3016\(84\)90379-1](https://doi.org/10.1016/0360-3016(84)90379-1).
 43. Lee, Jungnam, et al. "Laser Ablation of Pancreatic Cancer Using a Cylindrical Light Diffuser." *Lasers in Medical Science*, 2022, <https://doi.org/10.1007/s10103-022-03527-x>.
 44. Ahrar, Kamran, et al. "Preclinical Assessment of a 980-Nm Diode Laser Ablation System in a Large Animal Tumor Model." *Journal of Vascular and Interventional Radiology*, vol. 21, no. 4, 1 Apr. 2011, pp. 555–561., <https://doi.org/10.1016/j.jvir.2010.01.002>.
 45. Rastinehad, Ardeshir R., et al. "Gold Nanoshell-Localized Photothermal Ablation of Prostate Tumors in a Clinical Pilot Device Study." *Proceedings of the National Academy of*

- Sciences*, vol. 116, no. 37, 2019, pp. 18590–18596.,
<https://doi.org/10.1073/pnas.1906929116>.
46. “Wave Speeds.” *Hyperphysics*, Department of Physics and Astronomy Georgia State University, <http://hyperphysics.phy-astr.gsu.edu/hbase/Sound/souspe2.html>.
 47. “Stiffness — an Unknown World of Mechanical Science?” *Injury*, vol. 31, 1 Nov. 2001, pp. 14–84.,
[https://doi.org/10.1016/s0020-1383\(00\)80040-6](https://doi.org/10.1016/s0020-1383(00)80040-6).
 48. OpenStax. “University Physics Volume 1.” *17.2 Speed of Sound | University Physics Volume 1*, 3 Aug. 2016,
<https://courses.lumenlearning.com/suny-osuniversityphysics/chapter/17-2-speed-of-sound/>.
 49. Adiga, V. P., et al. “Temperature Dependence of Mechanical Stiffness and Dissipation in Ultrananocrystalline Diamond.” *SPIE Proceedings*, 2009,
<https://doi.org/10.1117/12.822795>.
 50. “Acoustic Impedance, Intensity and Power.” *Acoustic Impedance and Intensity: From Physclips Waves and Sound*,
<https://www.animations.physics.unsw.edu.au/jw/sound-impedance-intensity.htm>.
 51. “5-9 Acoustic Impedance - University of Wisconsin–Stevens ...” *Acoustic Impedance*, University of Wisconsin,
https://www4.uwsp.edu/physastr/kmanning/Phys115/Link5-09_acoustic_impedance.pdf.
 52. Dukhin, Andrei S., and Philip J. Goetz. “Fundamentals of Acoustics in Homogeneous Liquids.” *Characterization of Liquids, Nano- and Microparticulates, and Porous Bodies Using Ultrasound*, 7 June 2010, pp. 91–125.,
[https://doi.org/10.1016/s1383-7303\(10\)23003-x](https://doi.org/10.1016/s1383-7303(10)23003-x).
 53. “Ultrasound.” *National Institute of Biomedical Imaging and Bioengineering*, U.S. Department of Health and Human Services,
<https://www.nibib.nih.gov/science-education/science-topics/ultrasound>.
 54. Bühling, Benjamin, et al. “Enhancing the Spectral Signatures of Ultrasonic Fluidic Transducer Pulses for Improved Time-of-Flight Measurements.” *Ultrasonics*, vol. 119, 9 July 2022, p. 106612.,
<https://doi.org/10.1016/j.ultras.2021.106612>.
 55. Uematsu, Takayoshi, et al. “B-Mode Ultrasound Imaging, Doppler Imaging, and Real-Time Elastography in Cutaneous Malignant Melanoma and Lymph Node Metastases.” *Healthcare*, vol. 1, no. 1, 23 Oct. 2013, pp. 84–95.,
<https://doi.org/10.3390/healthcare1010084>.
 56. Grogan, Scott P. “Ultrasound Physics and Instrumentation.” *StatPearls [Internet]*, U.S. National Library of Medicine, 7 Apr. 2021,
<https://www.ncbi.nlm.nih.gov/books/NBK570593/>.
 57. Guerra, J. “Axial, Lateral, and Temporal Resolution in Ultrasound.” *Conquest Imaging*, MXR Imaging, 8 Feb. 2021,
<https://conquestimaging.com/ultrasound-blog/axial-lateral-and-temporal-resolution-in-ultrasound/>.
 58. Daneshvari Solanki, MD. “Regional Anesthesia Rotation.” *Ultrasound*, University of Texas Medical Branch,
https://www.utmb.edu/pedi_ed/adapt/LOs/Regional%20Anesthesia%20Rotation-%20original/page_10.htm#:~:text=Axial%20resolution%20is%20the%20ability,provide%20a%20better%20axial%20image.
 59. Ng, Alexander, and Justiaan Swanevelder. “Resolution in Ultrasound Imaging.” *Continuing Education in Anaesthesia Critical Care & Pain*, vol. 11, no. 5, 23 Aug. 2011, pp. 186–192.,
<https://doi.org/10.1093/bjaceaccp/mkr030>.
 60. Bushberg, Jerrold T., et al. *The Essential Physics of Medical Imaging*. Lippincott Williams & Wilkins, 2021.

61. “B Principles of Ultrasound - DC Conferences.” *Basic Physical Principles of Ultrasound*, DCC Conference Specialists, http://www.dconferences.com.au/lcmc2018/pdf/6._Basic_Principles_of_Ultrasound.pdf.
62. Handke, M. “Dynamic Changes of Atrial Septal Defect Area: New Insights by Three-Dimensional Volume-Rendered Echocardiography with High Temporal Resolution*.” *European Journal of Echocardiography*, vol. 2, no. 1, 1 Mar. 2001, pp. 46–51., <https://doi.org/10.1053/euje.2000.0064>.
63. Ng, Alexander, and Justiaan Swanevelder. “Resolution in Ultrasound Imaging.” *Continuing Education in Anaesthesia Critical Care & Pain*, vol. 11, no. 5, 13 Dec. 2017, pp. 186–192., <https://doi.org/10.1093/bjaceaccp/mkr030>.
64. Ng, Alexander, and Justiaan Swanevelder. “Resolution in Ultrasound Imaging.” *Continuing Education in Anaesthesia Critical Care & Pain*, vol. 11, no. 5, 23 Aug. 2011, pp. 186–192., <https://doi.org/10.1093/bjaceaccp/mkr030>.
65. Lee, Wonseok, and Yongrae Roh. “Ultrasonic Transducers for Medical Diagnostic Imaging.” *Biomedical Engineering Letters*, vol. 7, no. 2, 2017, pp. 91–97., <https://doi.org/10.1007/s13534-017-0021-8>.
66. GmbH, PI Ceramic. “Generating Ultrasound with Piezo Components.” *Piezo Ceramic Technology, Piezo Actuators & Piezo Components from PI Ceramic*, <https://www.piceramic.com/en/expertise/piezo-technology/generating-ultrasound-with-piezo-components/>.
67. Katzir, Shaul. “The Discovery of the PiezoElectric Effect.” *The Beginnings of Piezoelectricity a Study in Mundane Physics*, Springer, Dordrecht, 2006.
68. Company, A Johnson Electric. “The Piezoelectric Effect - Piezoelectric Motors & Motion Systems.” *Nanomotion*, Nanomotion, 28 Aug. 2018, [https://www.nanomotion.com/nanomotion-technology/piezoelectric-effect/#:~:text=One%20of%20the%20unique%20characteristics,an%20electric%20field%20is%20applied\)](https://www.nanomotion.com/nanomotion-technology/piezoelectric-effect/#:~:text=One%20of%20the%20unique%20characteristics,an%20electric%20field%20is%20applied)).
69. Amin Abas, Amry, et al. “Effect of Backing Layer Composition on ... - Inis.iaea.org.” *Effect of Backing Layer Composition on Ultrasonic Probe Bandwidth*, Malaysian Nuclear Agency, https://inis.iaea.org/collection/NCLCollectionStore/_Public/43/056/43056468.pdf.
70. Do Nascimento, Valeria M., et al. “Influence of Backing and Matching Layers in Ultrasound Transducer Performance.” *SPIE Proceedings*, 2003, <https://doi.org/10.1117/12.479924>.
71. Zhu, Jie, and Wenwu Cao. “Optimization of Matching Layer Design for Medical Ultrasonic Transducer.” *PennState*, Penn State University, 2008.
72. Rathod, Vivek T. “A Review of Acoustic Impedance Matching Techniques for Piezoelectric Sensors and Transducers.” *Sensors*, vol. 20, no. 14, 2020, p. 4051., <https://doi.org/10.3390/s20144051>.
73. Callens, Dorothee, et al. “Matching Ultrasonic Transducer Using Two Matching Layers Where One of Them Is Glue.” *NDT & E International*, vol. 37, no. 8, 18 Feb. 2004, pp. 591–596., <https://doi.org/10.1016/j.ndteint.2004.03.005>.
74. Gill, Brian. “Why Does an Ultrasound Probe Need Matching Layers?” *Probo Medical*, 25 Jan. 2022, <https://www.probomedical.com/learn/blog/why-does-an-ultrasound-probe-need-matching-layers/#:~:text=%E2%80%9CUltrasound%20probes%20typically%20are%20made,into%20the%20transducer%20for%20detection>.
75. Adams, Janet M. “Ultrasound Gel: A Necessary Mess.” *Cincinnati Children's Blog*, 12 Feb. 2019,

- <https://blog.cincinnatichildrens.org/radiology/ultrasound-gel-a-necessary-mess>.
76. Lewis, Matthew A., et al. "Thermometry and Ablation Monitoring with Ultrasound." *International Journal of Hyperthermia*, vol. 31, no. 2, 2015, pp. 163–181.,
<https://doi.org/10.3109/02656736.2015.1009180>.
 77. Varghese, T, et al. "Ultrasound Monitoring of Temperature Change during Radiofrequency Ablation: Preliminary in-Vivo Results." *Ultrasound in Medicine & Biology*, vol. 28, no. 3, 18 May 2002, pp. 321–329.,
[https://doi.org/10.1016/s0301-5629\(01\)00519-1](https://doi.org/10.1016/s0301-5629(01)00519-1).
 78. Mohana Shankar, P. "A General Statistical Model for Ultrasonic Backscattering from Tissues." *IEEE Transactions on Ultrasonics, Ferroelectrics and Frequency Control*, vol. 47, no. 3, May 2000, pp. 727–736.,
<https://doi.org/10.1109/58.842062>.
 79. Kiss, Miklos Z., et al. "Investigation of Temperature-Dependent Viscoelastic Properties of Thermal Lesions in Ex Vivo Animal Liver Tissue." *Journal of Biomechanics*, vol. 42, no. 8, 18 May 2009, pp. 959–966.,
<https://doi.org/10.1016/j.jbiomech.2009.03.002>.